IEEE Access
Multidisciplinary ⋮ Rapid Review ⋮ Open Access Journal

Received 2 January 2023, accepted 21 January 2023, date of publication 23 January 2023, date of current version 27 January 2023.

Digital Object Identifier 10.1109/ACCESS.2023.3239510

RESEARCH ARTICLE

Tunable Dual- and Multi-Channel Filter Based on Cantor Photonic Crystals Embedded With Graphene

XIAOLING CHEN[1,3], PU ZHANG[2], DONG ZHONG[1,3], (Member, IEEE), AND JUNJIE DONG[3]

[1]School of Electrical and Information Engineering, Hubei University of Science and Technology, Xianning 437100, China
[2]School of Education, Hubei University of Science and Technology, Xianning 437100, China
[3]Laboratory of Optoelectronic Information and Intelligent Control, Hubei University of Science and Technology, Xianning 437100, China

Corresponding authors: Pu Zhang (zhangpu@hbust.edu.cn) and Dong Zhong (zhongdong@hbust.edu.cn)

This work was supported in part by the National Natural Science Foundation of China (NSFC) under Grant 51975542, in part by the National Scientific Research Project Cultivation Program of Hubei University of Science and Technology under Grant 2021-23GP01, and in part by the Scientific Research Project of Hubei University of Science and Technology under Grant 2023-24X03 and Grant 2022-23X08.

ABSTRACT We theoretically investigate the tunable dual- and multi-channel filter in one-dimensional aperiodic photonic crystals (PCs) embedded with graphene. The dielectrics slabs arrayed alternately submit to the Cantor sequence rule and graphene sheets are local at the interfaces of dielectrics layers. Cantor PCs are fractal structures and support a series of discrete resonant channels in transmission spectra, *viz*. fractal states. Consequently, dual- and multi-filtering channels could be achieved in the compound systems. The central wavelength of each channel and its value of transmission could be modulating by the chemical potential of grapheme and the incident angle as well. It shows that the dual-channel amplitude of transmission can be varied by over 100% and the multiple channels could be switched on and off by the chemical potential of graphene. This study will be very helpful in designing tunable optical filters.

INDEX TERMS Cantor sequence, graphene, optical fractal, photonic crystal, photonic filter.

I. INTRODUCTION

Photonic technology has greatly revolutionized the optical communications in the past decades due to its tremendous progresses made. High speed, low loss, high performance, and reliable optical communication network has been realized through the photonic technology. One of the key components in optical communication systems is the optical filter, which is responsible for choosing specific wavelength of optical information to transmit or reflect.

Various schemes have so far been put forward for realizing the optical filters, among which photonic crystals (PCs) are the most popular ones. PCs [1], [2] are composed of periodic dielectric structures and possess a complete photonic band gap (PBG) in a certain frequency range. Once the frequency falls into the PBG, the propagation of light is strongly suppressed [3], [4]. Therefore, the filtering process can be easily realized, and the PBG can also be reconfigured to obtain filters with different spectral characteristics. In some applications, dynamic tunable filters with ultra-narrow bandpass are highly desirable for potential applications in high-precision optical sensing [5], dense wavelength division multiplexing [6], and wavelength-modulation spectroscopy [7]. On the other hand, quasi-periodic PCs have higher transmission efficiency, smaller band-width, and higher quality factor. Quasi-periodic PCs can support more defect cavities than the conventional periodic PCs [8], [9]. The defect cavities could induce the optical fractal effect in the PBG region. The optical fractal states are transmission modes of light waves. The transmission mode has a peak value of transmittance and a very low reflectivity in quasi-periodic PCs, which well meets the design requirements of the narrowband filters [10], [11], [12]. The properties of quasi-periodic PCs can be changed by certain deterministic rules, such as Fibonacci [13], Octonacci [14], Thue-Morse [15], Rudin-Shapiro [16], and

The associate editor coordinating the review of this manuscript and approving it for publication was Sukhdev Roy.

Cantor [17], [18], [19]. In addition, other studies conducted in the literature are also briefly discussed to show the importance of various quasi-periodic crystals [20], [21], [22]. However, once the photonic filter is constituted, the amplitude and center frequency of the channel may be permanently fixed, and cannot be conveniently and flexibly adjusted in some specific application scenarios.

Graphene is a two-dimensional lattice with perfect honeycomb structure, which has excellent conductivity and many extraordinary optical properties [23], [24], particularly the property of exciting surface polariton [25], [26]. The photonic crystals based on graphene have been extensively studied so far, such as oscillations [27], [28], supermodels [29], optical bistabilities [30], and optical modulators [31], [32]. In addition, the optical characteristic quantity is governed by the surface conductivity of graphene. The graphene surface conductivity is a function of the chemical potential. Generally, the chemical potential of graphene can be changed by loading an external grid voltage on it or by chemical doping [33]. This provides great convenience for graphene to modulate the optical properties induced by the graphene-based photonic crystals. Therefore, here we construct a complex system consisting of a one-dimensional quasi-periodic photonic crystal with graphene to realize a tunable dual-channel optical filter.

Tunable dual- and multi-channel optical filters are studied and numerically investigated in Cantor lattices embedded with graphene. The Cantor lattices are formed by two alternating dielectric slabs with different refractive indices and graphene is imbedded at the interfaces of these dielectric slabs. The discrete transmission channels and extension of channels by increasing the sequence number are demonstrated firstly. Subsequently, the tunability of filtering channels of optical waves is explored by changing the chemical potential of graphene and the incident angle of lights. In order to explore the channel regulation mechanism, the surface conductivity of graphene and the distribution of electric field are given as well. This work could be utilized for optical filters and optical modulators.

II. COMPLEX CANTOR LATTICE AND GRAPHENE

The one-dimensional quasi-periodic multilayers abiding by Cantor sequence are composed of two types of dielectrics A and B. The Cantor sequence submits to the substitution rule: $S_0 = A$, $S_1 = ABA$, $S_2 = ABABBBABA$, $S_3 = S_2(3B)^2S_2$, ……, $S_N = S_{N-1}(3B)^{N-1}S_{N-1}$, ……, where N ($N = 0, 1, 2, 3, \ldots\ldots$) is the generation number. Figure 1 gives diagram of Cantor dielectrics multilayers and graphene for different generation number N. For example, the complex structure can be expressed as ACBCACBCBCBCACBCA for $N = 2$.

The materials of A and B are represented as Si and SiO_2, respectively. The corresponding refractive indices are $n_A = 3.53$ and $n_B = 1.46$. The quasi-periodic system is placed in air and the refractive index of substrate surrounding is set as $n_0 = 1$. The thicknesses of dielectric slabs are one

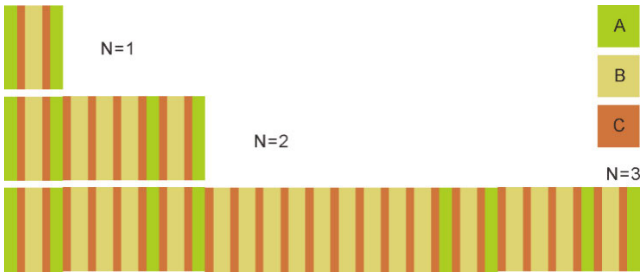

FIGURE 1. Diagram of the Cantor dielectric multilayers and graphene for $N = 1, 2, 3$, respectively. The symbol of N is the generation number of the Cantor sequence.

quarter of an optical wavelength, viz. $d_A = \lambda_0/4/n_A = 0.1098\ \mu$m, $d_B = \lambda_0/4/n_B = 0.2654\ \mu$m, where $\lambda_0 = 1.55\ \mu$m is the central wavelength. The graphene, denoted by layer C, is embedded arbitrary two dielectrics. Graphene is considered as a metal element in the near-infrared band, and is usually regarded as an ultra-thin two-dimensional dielectric with unique conductivity and equivalent thickness of d_g.

The equivalent dielectric constant of graphene is expressed as

$$\varepsilon_g = 1 + i\frac{\sigma\eta_0}{k_0 d_g}. \tag{1}$$

Here, the symbol i denotes the imaginary unit, k_0 represents the wave vector in vacuum, η_0 is the vacuum resistivity parameter in vacuum. The refractive index of graphene can be characterized by its conductivity as $n_g = \sqrt{\varepsilon}_g$. The conductivity of graphene can be obtained from the Kubo formula [33], [34], which could be written as

$$\begin{aligned}\sigma(\omega, \mu_c, \tau, T_b) = &-\frac{ie(\omega + i\tau^{-1})^2}{\pi\hbar^2} \\ &\times \Big[\int_{-\infty}^{+\infty} \frac{|\varepsilon|}{(\omega + i\tau^{-1})^2}\frac{\partial f_d(\varepsilon)}{\partial\varepsilon}d\varepsilon \\ &- \int_{-\infty}^{+\infty} \frac{\partial f_d(-\varepsilon) - \partial f_d(\varepsilon)}{(\omega + i\tau^{-1})^2 - 4(\varepsilon/\hbar)^2}d\varepsilon\Big]\end{aligned} \tag{2}$$

where $f_d = 1/(1 + \exp[(\varepsilon - \mu_c)/K_B T_b])$ is the Fermi-Dirac distribution function. $\varepsilon, \mu_c, \omega$ represent the particle energy, the chemical potential of graphene, the angular frequency, respectively. $e, K_B, \hbar$ denote the electron element charge, and the Boltzmann's constant, the reduced Plank's constant, respectively. The environment temperature is set as $T_b = 300$ K and the relaxation time is set as $\tau = 0.5$ ps.

The first term and the second term of Equation (2) can be simplified to

$$\sigma_{intra} = i\frac{e^2 k_B T_b}{\pi\hbar^2(\omega + i\tau^{-1})}\Big[\frac{\mu_c}{k_B T_b} + 2\ln(\exp(-\frac{\mu_c}{k_B T_b}) + 1)\Big], \tag{3}$$

and

$$\sigma_{inter} = i\frac{e^2}{4\pi\hbar}\ln\Big[\frac{2|\mu_c| - \hbar(\omega + i\tau^{-1})}{2|\mu_c| + \hbar(\omega + i\tau^{-1})}\Big], \tag{4}$$

respectively. Both interband and intraband transitions involve μ_c and ω. In other words, the surface conductivity of graphene is a function of chemical potential and light incidence frequency. In the THz band, the interband transition is dominant because the excitation photon energy $\hbar\omega$ is less than $2\mu_c$, and the optical property of graphene is analogue to metals.

The one-dimensional photonic multi players embedded by graphene arranges along the horizontal direction. Considering a light impinges on the structure from the left and transmits from the right and ignoring the nonlinear effect of light, we use the transmission matrix method, the transfer matrix of dielectric sheet can be expressed as

$$M_j = \begin{bmatrix} \cos\varsigma_j & -\frac{i}{\eta_j}\sin\varsigma_j \\ -i\eta_j \sin\varsigma_j & \cos\varsigma_j \end{bmatrix}, \tag{5}$$

where $\varsigma_j = 2\pi n_j d_j \cos\theta_j/\lambda$. n_j, d_j and θ_j are the refractive index, the dielectric thickness, and the incident angle respectively. The modified admittance for a transverse magnetic (TM) wave is given by $\eta_j = (\varepsilon_0\varepsilon_r)^{1/2}/[(\mu_0\mu_r)^{1/2}\cos\theta_j]$. The total transfer matrix of the complex structure is obtained by $M = M_1\ M_2 \ldots M_j = [m_{11}, m_{12}; m_{21}, m_{22}]$. Therefore, for a TM polarized wave polarized wave, the transmission coefficients T can be obtained by transfer matrix

$$T = \frac{2\eta_0}{(m_{11} + m_{12}\eta_{N+1})\,\eta_0 + (m_{21} + m_{22}\eta_{N+1})}\frac{\cos\theta_1}{\cos\theta_{N+1}}. \tag{6}$$

The chemical potential of graphene is a Femi level, so the chemical potential can be controlled by chemical doping or the external grid voltage on graphene. As the voltage load on graphene is positive, the chemical potential of graphene increases, while the voltage load on graphene is negative, the chemical potential decreases. Therefore, the surface conductivity of graphene can be flexibly adjusted by the bias voltage on graphene. Graphene is treated as a thin film with an equivalent thickness. Equivalent refractive index of dielectric is a function of the chemical potential of graphene. Therefore, the refractive index of the equivalent dielectric can be flexibly controlled by the chemical potential of graphene. If graphene is embedded into the photonic crystal, the existence of graphene will affect the overall transmittance of the structure, and the surface conductivity of graphene is a chemical potential function, which can change the transmission spectrum of the entire composite structure through the chemical potential of graphene, and finally regulate the central frequency of resonant modes in the structure.

The relation between the chemical potential μ_c and the applied gate voltage V_g on graphene can be expressed as

$$|\mu_c| = \hbar v_F \sqrt{\pi\left|a_0\left(V_g - V_D\right)\right|}, \tag{7}$$

where the parameter a_0 is empirical constant and is given by $a_0 = 9 \times 10^{-16}$ m, $v_F \approx 10^6$ m/s is the Fermi velocity of electrons in graphene, and V_D is the offset bias voltage and it is generally set as $V_D = 0$ for intrinsic graphene.

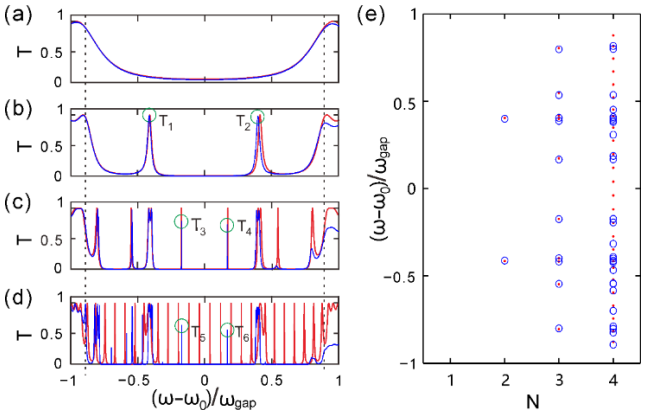

FIGURE 2. (a-d) Transmission spectra of light waves in Cantor PCs with or without graphene for the generation number $N = 1, 2, 3$ and 4, respectively. The red line represents the transmission spectra of the structure. The blue line represents the transmission spectra of the structure composed of graphene. (e) Distribution of optical fractal states in the normalized frequency of the Cantor PCs with or without graphene for the generation number $N = 1, 2, 3$ and 4, respectively. The graphene chemical potential is $\mu_c = 0.5$ eV.

III. NUMERICAL RESULTS AND DISCUSSIONS

For a TM wave, as it normally impinges on the quasi-periodic photonic crystal multilayers abiding by Cantor sequence and graphene from the left. Figure 2(a-d) respectively give the light transmission spectra of Cantor photonic multilayers with or without graphene for the generation number $N = 1, 2, 3$ and 4. The graphene chemical potential is given by $\mu_c = 0.5$ eV. The horizontal coordinate is the normalized frequency of the incidence $(\omega - \omega_0)/\omega_{gap}$. Here, ω_{gap} is the photonic bandgap expressed as $\omega_{gap} = 4\omega_0 \arcsin|[\mathrm{Re}(n_B) - \mathrm{Re}(n_A)]/[\mathrm{Re}(n_A) + \mathrm{Re}(n_B)]|^2/\pi$, $\omega_0 = 2\pi c/\lambda_0$is called as the central frequency of incidence. ω_{gap} is a typical important parameter to characterize photonic crystals. The real term of the material refractive index determines the propagation phase of the traveling wave, and ultimately determines the resonant wavelength of the transmission mode. In addition, the photonic band gap ω_{gap} of photonic crystals is also determined by the real term of the material refractive index. Within the dotted line range marked in Figure 2(a-d), one can see that there are 0, 2, 10, 26 resonant states in red curves as the generation number increases from 1 to 4. These resonances are symmetrically distributed around the center and their peak values are all 1. The number of transmission modes increases exponentially with the generation number of dielectric sequence. As graphene sheets are imbedded at the interfaces of slabs, the spectrum on the left side of the center point shifts slightly to the right, while the spectrum on the right side of the center point shifts slightly to the left. In the first three generations of the iterative sequence, the total number of resonance peaks remains unchanged. Since the fourth generation, the total number has changed.

As a light wave illuminates normally on the photonic quasicrystals, defects in Cantor PCs can induce optical fractal states. The optical fractal states correspond to a series

of transmission modes. The bandgap in the transmission spectrum can naturally be used as photonic filters by analogy with the energy band structure of electrons in semiconductors. Hence, dual- and multi-filtering channels could be achieved for appropriate iteration sequence.

Figure 2(e) shows the positions of optical fractal resonant states in the normalized frequency for different generation number. As the generation number increases, it is observed that the fractal states of the Cantor PCs with or without graphene split and increase exponentially. The number of optical fractal states in Cantor PCs embedded in graphene is the same as that in the Cantor PCs for the generation number $N = 1, 2, 3$. The position of the blue circle is offset relative to the red dot. For $N = 4$, the total number of red circles is 26, while the total number of blue circles is 29. The optical fractal states (in blue circle) split to forms new optical fractal states in the normalized frequency range of $(\omega - \omega_0)/\omega_{\text{gap}} = [-0.46, -0.41]$ and $(\omega - \omega_0)/\omega_{\text{gap}} = [0.34, 0.41]$, and the optical fractal states severely degrade or even disappear in the normalized frequency range of $(\omega - \omega_0)/\omega_{\text{gap}} = [-0.35, 0.35]$ and $(\omega - \omega_0)/\omega_{\text{gap}} = [0.45, 0.54]$. And apparently, the scalability of the filter channels can be adjusted by controlling the generation number, the central wavelength of each channel and its value of transmission could be modulating by the chemical potential of graphene.

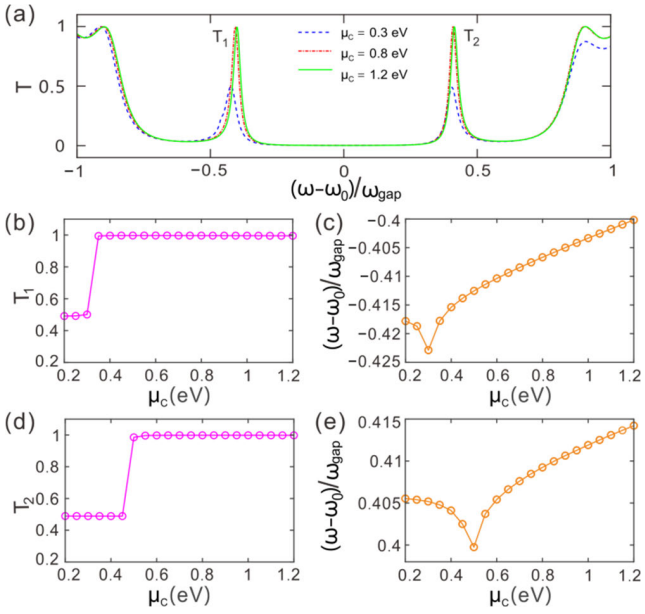

FIGURE 3. (a) Transmission spectra varying with the frequency of the incident light wave for different graphene chemical potentials. (b), (d) Transmittance versus chemical potential for the two filter channels. (c), (e) Central frequency of the two filter channels for different chemical potential. Here, the generation number is $N = 2$ and the incidence wavelength is $\lambda = 1.55$ μm.

Figure 3(a) provides the transmission spectra for $\mu_c = 0.3$, 0.8 and 1.2 eV. One can see that there is a photonic band gap in the transmission curve, of which two resonance peaks are induced, and they correspond to two filter channels. With the different chemical potential of graphene, the transmission peaks of the two resonance modes are different, and the center frequencies of the resonance peak move slightly. For $\mu_c = 0.3$ eV, the transmission peaks of these two channels are 0.501 and 0.4892, respectively. The corresponding horizontal coordinates are -0.423 and 0.4053. For $\mu_c = 0.8$ eV, the left peak transmittance is $T = 0.9965$ at the normalized frequency $(\omega - \omega_0)/\omega_{\text{gap}} = -0.4065$, the right peak transmittance is $T = 0.9981$ at the normalized frequency $(\omega - \omega_0)/\omega_{\text{gap}} = 0.4093$. For $\mu_c = 1.2$ eV, the parameters are $T = 0.9951$ at $(\omega - \omega_0)/\omega_{\text{gap}} = -0.4$, and $T = 0.9978$ at $(\omega - \omega_0)/\omega_{\text{gap}} = 0.4143$ respectively. Significantly, for $\mu_c = 0.8$ and 1.2 eV, the transmission values of the left and right peaks are close to 1. For a dual channel filter, it is feasible to adjust the central wavelengths and the resonant peak values of the channels through the chemical potential of graphene.

In order to demonstrate how graphene sheets modulate the transmission performance and the center frequency of the filter channel, we sampled the channels where the channels in the middle of the band gap are marked as T_1, T_2, and the corresponding central frequencies are ω_1, ω_2, respectively. Figure 3(b-e) show the transmittance and the normalized frequency of the channel versus the graphene chemical potential for a center wavelength. One can see that the chemical potential of graphene is less than or equal to 0.3 eV, the transmittance T_1 equals to 0.5, and while it exceeds 0.35 eV, the value rapidly steps up to one as shown in Figure 3(b). In Figure 3(c), as μ_c is less than or equal to 0.3 eV, the center frequency of the transmission mode decreases with the increase of the chemical potential of graphene. As μ_c exceeds 0.3 eV, the center frequency of the transmission mode increases with the increase of the chemical potential of graphene. The center frequency of the transmission mode is the minimum at the chemical potential of 0.3 eV. Similarly, this trend also exists for the other channel. In Figure 3(d), by increasing the chemical potential of graphene to 0.45 eV, the transmittance T_2 remains 0.5, and while it exceeds 0.5 eV, the value rapidly steps up to one. The center frequency of the transmission mode decreases first and then increases with the increase of graphene value as shown in Figure 3(e). The central frequency of the transmission mode is the minimum for $\mu_c = 0.45$ eV. It is not difficult to find that a small change in the graphene value will cause a change in the central frequency of the transmission mode. In addition, the transmittance of the transmission mode changes significantly if and only if the value of graphene increases to a certain value, and the maximum transmittance is close to 1. It shows that the dual-channel amplitude of transmission can be varied by over 100%.

Figure 4(a) presents the real part of surface conductivity $\text{Re}(\sigma)$ for different values of chemical potential. For three given values of $\mu_c = 0.3$, 0.4 and 0.5 eV, there are three curves, correspondingly, of $\text{Re}(\sigma)$ as the normalized frequency changes. For a fixed value of graphene chemical potential, viz $\mu_c = 0.3$ eV, the real part of the surface conductivity of graphene is close to 0.6×10^{-5} S and keeps constant as the normalized frequency $(\omega - \omega_0)/\omega_{\text{gap}}$ is in

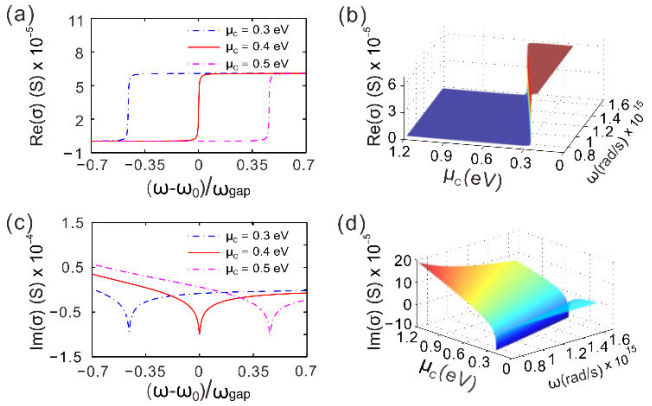

FIGURE 4. (a), (c) Real part and imaginary part of graphene surface conductivity varying with the normalized frequency for different values of chemical potential, respectively. (b), (d) Real part and imaginary part of graphene surface conductivity by modulating simultaneously the incident frequency and chemical potential, respectively.

the range of $(-0.418, 0.7)$. While in the range of $(-0.7, -0.418)$, the value sharply jumps down to zero. As μ_c increases to 0.4 eV and 0.5 eV, the curve shifts to the right overall, the normalized frequency at the jump is $(\omega - \omega_0)/\omega_{gap} = 0.067$ and $(\omega - \omega_0)/\omega_{gap} = 0.544$ respectively, and the corresponding $\mathrm{Re}(\sigma)$ in each curve is 0.6×10^{-5} S. The parameter $\mathrm{Re}(\sigma)$ is the counterpart of the imaginary part of the graphene equivalent dielectric constant $\mathrm{Im}(\varepsilon_g)$, this indicates the optical loss in graphene. Larger $\mathrm{Re}(\sigma)$ means greater loss and weaker transmitted intensity. As graphene is adjusted to a certain range, the optical loss remains unchanged, and the corresponding transmittance value could not decay, close to 1. This approves the phenomenon that the transmittance changes with the normalized frequency of incident light for different chemical potential as shown in Figure 3(a). Therefore, this characteristic can be used for manipulating the channel frequency.

Figure 4(b) provides the real part of surface conductivity $\mathrm{Re}(\sigma)$ of the photonic lattice. The parameters space is composed of μ_c and incident frequency ω. One can see that, the value of $\mathrm{Re}(\sigma)$ remains constant by raising the graphene chemical potential to a certain value, and keeping on increasing the graphene chemical potential or turning up the incident frequency. Since $\mathrm{Re}(\sigma)$ dominates the loss in graphene of light, changing μ_c or modulating ω is an important step to control the propagation of light in complex multilayer. The jump of this turning point, that is, the abrupt increase of $\mathrm{Re}(\sigma)$ from zero to a certain value, is the result of electron transition from intraband to interband in graphene.

Figure 4(c) gives the imaginary part of surface conductivity $\mathrm{Im}(\sigma)$ varying with μ_c. The whole curve of $\mathrm{Im}(\sigma)$ moves to the right as the chemical potential increases. By increasing the frequency of light, there is an inflection point of each curve, on the left side of the inflection point, $\mathrm{Im}(\sigma)$ decreases, and then increases smoothly to a constant value as the frequency passes the inflection point. The parameter of $\mathrm{Im}(\sigma)$ determines the real part of graphene equivalent permittivity and $\mathrm{Im}(\sigma)$ can be modulated by μ_c, so we can flexibly adjust the transmittance through the chemical potential of graphene.

We continuously adjust the graphene chemical potential and depict the imaginary part of surface conductivity $\mathrm{Im}(\sigma)$ varying with the incident frequency in the parameter space as shown in Figure 4(d). It demonstrates that $\mathrm{Im}(\sigma)$ produces an effect after the graphene chemical potential increases to a certain value, and shows a trend of decreasing rapidly and then increasing to a certain value in the incident frequency. $\mathrm{Im}(\sigma)$ determines the real part of graphene equivalent permittivity, and graphene chemical potential can change the value of $\mathrm{Im}(\sigma)$, so we can flexibly adjust the transmittance through the chemical potential of graphene.

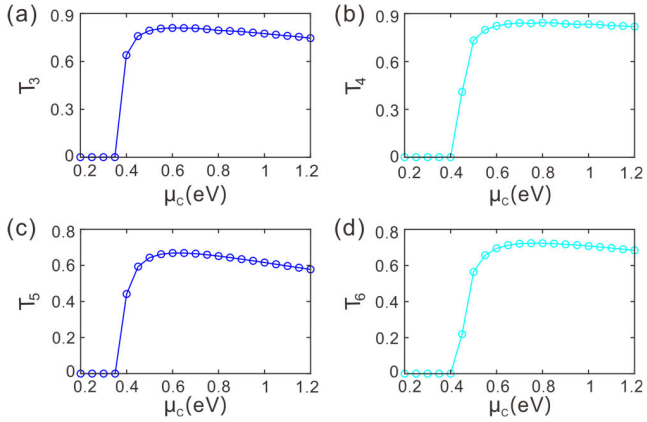

FIGURE 5. Transmittance of the channel versus chemical potential for the generation number $N = 3$ and 4, respectively.

Figure 5 explores the regulatory effect of graphene on channels in other sequences, *viz.* T_3, T_4, T_5 and T_6 (marked as O in Figure 2). One can see that the transmittances of channel are different for different μ_c. In Figure 5(a-b), the generation number N is set as 3, as $\mu_c \leq 0.35$ eV, the transmittance T_3 is equal to 0.0007. While $\mu_c = 0.4$ eV, the transmittance jumps to 0.639. The transmittance reaches the maximum 0.8093 at $\mu_c = 0.6$ eV. The transmittance decreases with the increase of the chemical potential as $\mu_c > 0.6$ eV. For the channel of T_4, the transmittance T_4 is close to 0.0007 as $\mu_c \leq 0.4$ eV. In the range of (0.45 eV, 0.8 eV), the transmission value of light waves increases with the chemical potential of graphene. The maximum transmittance is $T_m = 0.8428$ for T_4 around $\mu_c = 0.8$ eV, and then the transmittance T_4 decreases with the increase in μ_c.

The transmittance of T_5 changing with the chemical potential could be observed in Figure 5(c). In the chemical potential range of (0.2 eV, 0.35 eV), the maximum transmittance of T_5 approximates to zero. There is abrupt step of channel transmittance of $T_5 = 0.049$ at $\mu_c = 0.4$ eV and the value of transmission rises to 0.4413. The maximum transmittance of T_5 is $T_m = 0.685$ at $\mu_c = 0.6$ eV. Compared with T_3, the value of T_5 and its maximum are all decrease. In Figure 5(d), obviously, the transmittance T_6 is zero as $\mu_c \leq 0.4$ eV and rapidly increases as μ_c is in the range of (0.4 eV, 0.75 eV) and the maximum transmittance rises to the value of 0.7233 at

$\mu_c = 0.75$ eV. Therefore, the transmittance can be tuned by the chemical potential in the application of photonic filters. But if we want to get a dual-channel filter, and apply photonic crystals with different sequence, the graphene should be modulated in a compromise range. It shows that the multiple channels could be switched on and off by the chemical potential of graphene.

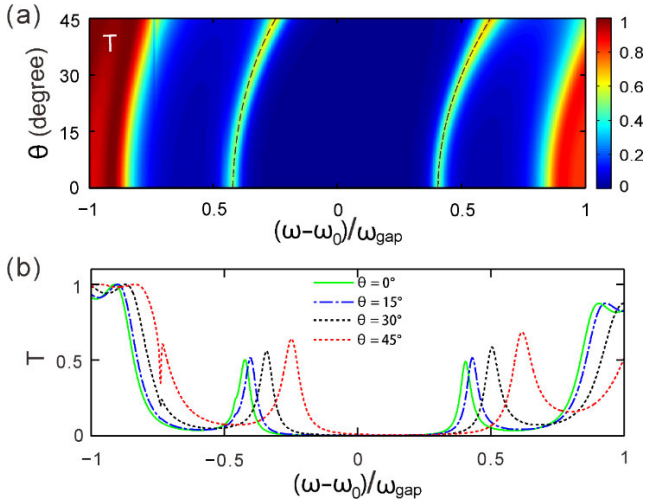

FIGURE 6. (a) Transmittance in the parameter space composed of the incident angle and the normalized frequency. (b) Transmission spectra for different incident angles. Here, the generation number is $N = 2$ and the graphene chemical potential is $\mu_c = 0.3$ eV.

Figure 6(a) gives the transmittance in the parameter space. The parameter space is composed of the incident angle and the normalized frequency $(\omega - \omega_0)/\omega_{gap}$. One can see that there are two defect modes in the parameter space. With the increase of frequency, no new defect modes appear. With the change of the incident angle, the defect mode moves along the dotted line in the parameter space. For each defect mode, the transmittance increases slightly with the increase of the incident angle, and the profile of the defect mode moves to a higher central frequency.

Figure 6(b) presents the transmission spectra for four given incident angles. One can see that the spectrum profile moves rightwards overall by increasing the incident angle. The normalized frequency of the resonant defect modes is higher for a larger incident angle and the transmission values of the peaks are higher relatively. Therefore, using the composite structure as a dual-channel photonic filter, the transmittance and center frequency of the filter channel can be flexibly adjusted through the chemical potential of graphene and the incident angle of light waves.

As mentioned above, there are two transmission peaks (denoted by T_1 and T_2) for $N = 2$. The corresponding wavelengths are the values of $\lambda_1 = 1.999$ and $\lambda_2 = 1.273$ μm, respectively. Here, we use the inverse transmission matrix method (in blue curve) and the finite difference time domain (in color bar) [33] method to simulate the electric field distribution, and the results of the two methods are consistent. For the light beams normally incident from the left, the Z-component of electric field intensity of T_1 for the Cantor lattices is given in Figure 7(a). One can see that the electric field intensity is mainly localized at the center of the defect B and attenuates from the center to the left and right. The localization of electric field manifests that the transmission peak is a resonant state. The electric field distribution at the peak of T_2 is given in Figure 7(b). The two largest distributions of electric field appear in defect layers BBB. This phenomenon also supports the characteristics of electric field localization, which indicates that the transmission peak is also a resonant mode. The above characteristic is necessary to realize dual-filtering channels.

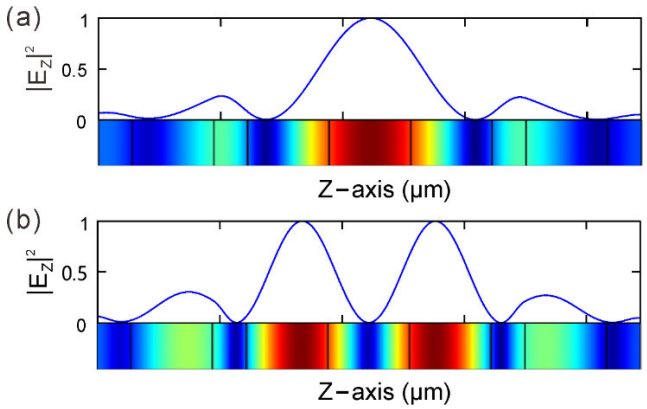

FIGURE 7. Mode field distribution of the light incident wavelength $\lambda_1 = 1.999$ and $\lambda_2 = 1.273$ μm, respectively. The generation number is $N = 2$, the incident angle is $\theta = 0°$ and the graphene chemical potential is $\mu_c = 0.3$ eV.

The distributions of electric fields are simulated using the software COMSOL and MATLAB as shown in Figure 7. The other results are calculated by MATLAB programs. The software of CorelDRAW is used to edit the figures.

Hyperbolic metamaterials composed by graphene and dielectric multilayers can support a Fabry–Perot resonant mode and the central wavelength of resonance could be modulated by the chemical potential of graphene and the thickness of dielectric [35]. Metamaterial terahertz filters have been achieved by periodic metallic rings with gaps. Graphene stripes are local at these gaps and the resonance frequency of the system can be altered by 40% by tuning the conductivity of graphene [36]. Graphene can also be utilized for tuning the reflection of lightwaves and it shows that the dual-band amplitude of reflection can be varied by over 15% and resonant positions can be shifted by over 90 cm^{-1} [37]. Furthermore, the composite structure of photonic crystal and graphene can realize the optical regulation of terahertz band [38], [39], [40]. We here investigate the dual- and multi-channel filter of transmission based on optical fractal resonances in quasi-periodic crystals, of which graphene is embedded at the position of the strongest local electric field. Therefore, the transmittance and the central wavelength of resonance can be greatly modulated by the chemical potential of graphene. It manifests that the dual-channel amplitude of transmission can be modulated by over 100% and the

multiple channels of filters could be switched on and off by the chemical potential of graphene in our systems.

IV. CONCLUSION

In summary, tunable dual- and multi-channel filter are investigated in one-dimensional aperiodic photonic crystals (PCs) embedded with graphene. The aperiodic PCs composed of two different dielectric slabs submit to the Cantor sequence law. The Cantor PCs can support a series of discrete resonant channels in transmission spectra, which provides the condition to realize dual- and multi-filtering channels. The central wavelength of each channel and its value of transmission could be modulated by changing the graphene chemical potential. The dual-channel amplitude of transmission can be changed by over 100% and the multiple channels could be turned on and off by the chemical potential of graphene. Moreover, the value of transmission increases and the central wavelength of the filter channel moves toward the short-wave direction as the incident angle is turned up. The study could provide a feasible scheme for tunable optical filters.

CONFLICT OF INTEREST

The authors declare that they have no conflict of interest.

REFERENCES

[1] M. Gryga, D. Ciprian, L. Gembalova, and P. Hlubina, "Sensing based on Bloch surface wave and self-referenced guided mode resonances employing a one-dimensional photonic crystal," *Opt. Exp.*, vol. 29, no. 9, pp. 12996–13010, Mar. 2021.

[2] F. Segovia-Chaves and H. Vinck-Posada, "The effect of the hydrostatic pressure and temperature on the defect mode in the band structure of one-dimensional photonic crystal," *Optik*, vol. 156, pp. 981–987, Mar. 2018.

[3] J. Joannopoulos, R. D. Meade, and J. N. Winn, *Photonic Crystals: Molding the Flow of Light*, 2nd ed. Princeton, NJ, USA: Princeton Univ. Press, 2007, ch. 1, sec. 4, pp. 44–49. [Online]. Available: http://press.princeton.edu/chapters/s8696.pdf

[4] A. Biswal, R. Kumar, C. Nayak, and S. Dhanalakshmi, "Photonic bandgap characteristics of GaAs/AlAs-based one-dimensional quasi-periodic photonic crystal," *Optik*, vol. 234, May 2021, Art. no. 166597.

[5] L. Kong, Y. Zhu, Y. Song, and J. Yang, "Beam steering approach for high-precision spatial light modulators," *Chin. Opt. Lett.*, vol. 8, no. 11, pp. 1085–1089, 2010.

[6] D. Sharma and Y. K. Prajapati, "Performance analysis of DWDM system for different modulation schemes using variations in channel spacing," *J. Opt. Commun.*, vol. 37, no. 4, pp. 401–413, Jan. 2016.

[7] M. R. Chaudhry, M. Zakwan, M. C. Onbasli, and A. Serpenguzel, "Symmetric meandering distributed feedback structures for silicon photonic circuits," *IEEE J. Sel. Topics Quantum Electron.*, vol. 26, no. 2, pp. 1–5, Mar. 2020.

[8] J. Wu, "TPP-assisted multi-band absorption enhancement in graphene based on Fibonacci quasiperiodic photonic crystal," *Results Phys.*, vol. 33, Feb. 2022, Art. no. 105210.

[9] M. Bellingeri, A. Chiasera, I. Kriegel, and F. Scotognella, "Optical properties of periodic, quasi-periodic, and disordered one-dimensional photonic structures," *Opt. Mater.*, vol. 72, pp. 403–421, Oct. 2017.

[10] Y. Trabelsi, N. B. Ali, and M. Kanzari, "Tunable narrowband optical filters using superconductor/dielectric generalized thue-morse photonic crystals," *Microelectron. Eng.*, vol. 213, pp. 41–46, May 2019.

[11] Y. Wu, W. Wu, and J. Hu, "Tunable perfect dual-narrowband absorber based on graphene-photonic crystal heterostructure," *Results Phys.*, vol. 34, Mar. 2022, Art. no. 105234.

[12] Y. Dai, B. Liu, S. Wang, K. Kong, and C. Chen, "A tunable dual-narrowband band-pass filter using plasma quantum well structure," *Results Phys.*, vol. 23, no. 6, pp. 370–374, 2014.

[13] F. Segovia-Chaves, H. Vinck-Posada, Y. Trabelsi, and N. B. Ali, "Transmittance spectrum in a one-dimensional photonic crystal with Fibonacci sequence superconductor–semiconductor," *Optik*, vol. 217, Sep. 2020, Art. no. 164803.

[14] E. F. Silva, C. H. Costa, M. S. Vasconcelos, and D. H. A. L. Anselmo, "Transmission spectra in graphene-based octonacci one-dimensional photonic quasicrystals," *Opt. Mater.*, vol. 89, pp. 623–629, Mar. 2019.

[15] H. Ni, J. Wang, and A. Wu, "Optical bistability in aperiodic multilayer composed of graphene and Thue-Morse lattices," *Optik*, vol. 242, Sep. 2021, Art. no. 167163.

[16] F. Segovia-Chaves and H. A. Elsayed, "Transmittance spectrum in a rudin Shapiro quasiperiodic one-dimensional photonic crystal with superconducting layers," *Phys. C, Supercond. Appl.*, vol. 587, Aug. 2021, Art. no. 1353898.

[17] S. Sahel, R. Amri, L. Bouaziz, D. Gamra, M. Lejeune, M. Benlahsen, K. Zellama, and H. Bouchriha, "Optical filters using Cantor quasi-periodic one dimensional photonic crystal based on Si/SiO_2," *Superlattices Microstruct.*, vol. 97, pp. 429–438, Sep. 2016.

[18] T.-C. King and Y.-M. Dong, "Unidirectional absorption properties in a defective semiconductor-dielectric asymmetric triadic Cantor photonic crystal," *Phys. E, Low-Dimensional Syst. Nanostruct.*, vol. 108, pp. 135–138, Apr. 2019.

[19] X. Chen, H. Ni, D. Zhao, and Y. Wang, "Optical fractal resonances in Cantor-like photonic crystals," *Appl. Opt.*, vol. 61, no. 26, pp. 7786–7792, 2022.

[20] S. A. Taya, A. A. Alkanoo, N. R. Ramanujam, P. Mahalakshmi, and D. Vigneswaran, "Photonic crystal with epsilon negative and double negative materials as an optical sensor," *Opt. Quantum Electron.*, vol. 50, no. 5, pp. 1–11, May 2018.

[21] N. R. Ramanujam, S. K. Patel, N. M. Reddy, S. A. Taya, D. Vigneswaran, and M. S. M. Rajan, "One-dimensional ring mirror-defect photonic crystal for detection of mycobacterium tuberculosis bacteria," *Optik*, vol. 219, Oct. 2020, Art. no. 165097.

[22] N. Kumar, Sonika, B. Suthar, and A. Rostami, "Novel optical behaviors of metamaterial and polymer-based ternary photonic crystal with lossless and lossy features," *Opt. Commun.*, vol. 529, Feb. 2023, Art. no. 129073.

[23] A. K. Geim and K. S. Novoselov, "The rise of graphene," *Nature Mater.*, vol. 6, pp. 183–191, Mar. 2007.

[24] K. Zhang, "Optical bistability in graphene-wrapped dielectric nanowires," *Opt. Exp.*, vol. 25, no. 12, pp. 13747–13759, Jun. 2017.

[25] I. Vitoria, C. R. Zamarreño, A. Ozcariz, J. J. Imas, I. del Villar, and I. R. Matias, "Surface exciton polariton resonances (SEPR)–based sensors," *Opt. Lasers Eng.*, vol. 160, Jan. 2023, Art. no. 107273.

[26] S. O. Abdol, B. Abdollahipour, and A. S. Vala, "Surface plasmon polaritons in a waveguide composed of weyl and dirac semimetals," *Opt. Mater.*, vol. 117, Jul. 2021, Art. no. 111213.

[27] F. Wang, C. Qin, B. Wang, H. Long, K. Wang, and P. Lu, "Rabi oscillations of plasmonic supermodes in graphene multilayer arrays," *IEEE J. Sel. Topics Quantum Electron.*, vol. 23, no. 1, pp. 125–129, Jan. 2017.

[28] F. Wang, C. Qin, B. Wang, S. Ke, H. Long, K. Wang, and P. Lu, "Rabi oscillations of surface plasmon polaritons in graphene-pair arrays," *Opt. Exp.*, vol. 23, pp. 31136–31143, Nov. 2015.

[29] H. Huang, H. Long, P. Lu, C. Qin, K. Wang, and B. Wang, "Low-loss plasmonic supermodes in graphene multilayers," *Opt. Exp.*, vol. 21, pp. 25324–25332, Oct. 2022.

[30] J. Wang, F. Xu, F. Liu, and D. Zhao, "Optical bistable and multistable phenomena in aperiodic multilayer structures with graphene," *Opt. Mater.*, vol. 119, Sep. 2021, Art. no. 111395.

[31] J. Gosciniak, D. T. H. Tan, and B. Corbett, "Enhanced performance of graphene-based electro-absorption waveguide modulators by engineered optical modes," *J. Phys. D, Appl. Phys.*, vol. 48, no. 23, Jun. 2015, Art. no. 235101.

[32] S. Luo, Y. Wang, X. Tong, and Z. Wang, "Graphene-based optical modulators," *Nanosc. Res. Lett.*, vol. 10, no. 1, pp. 1–11, Dec. 2015.

[33] D. Zhao, L. Wang, F. Liu, D. Zhong, and M. Wu, "Photonic stopband filters based on graphene-pair arrays," *Appl. Sci.*, vol. 11, no. 23, p. 11557, Dec. 2021.

[34] D. Zhao, S. Ke, Y. Hu, Y. Wang, and P. Lu, "Optical bistability of graphene embedded in parity-time-symmetric photonic lattices," *J. Opt. Soc. Amer. B, Opt. Phys.*, vol. 36, pp. 1731–1737, Jul. 2019.

[35] M. Dudek, R. Kowerdziej, A. Pianelli, and J. Parka, "Graphene-based tunable hyperbolic microcavity," *Sci. Rep.*, vol. 11, no. 1, p. 74, Jan. 2021.
[36] Y. Kai, S. Liu, S. Arezoomandan, A. Nahata, and B. Sensale-Rodriguez, "Graphene-based tunable metamaterial terahertz filters," *Appl. Phys. Lett.*, vol. 105, no. 9, 2014, Art. no. 093105.
[37] M. D. Goldflam, I. Ruiz, S. W. Howell, J. R. Wendt, M. B. Sinclair, D. W. Peters, and T. E. Beechem, "Tunable dual-band graphene-based infrared reflectance filter," *Opt. Exp.*, vol. 26, no. 7, pp. 8532–8541, 2018.
[38] L.-A. Bian, P. Liu, and G. Li, "Design of tunable devices using one-dimensional Fibonacci photonic crystals incorporating graphene at terahertz frequencies," *Superlattices Microstruct.*, vol. 98, pp. 522–534, Oct. 2016.
[39] Y. Li, L. Qi, J. Yu, Z. Chen, Y. Yao, and X. Liu, "One-dimensional multiband terahertz graphene photonic crystal filters," *Opt. Mater. Exp.*, vol. 7, no. 4, pp. 1228–1239, 2017.
[40] W. Belhadj and A. N. Al-Ahmadi, "Tunable narrowband terahertz multichannel filter based on one-dimensional graphene-dielectric photonic crystal," *Opt. Quantum Electron.*, vol. 53, no. 1, pp. 1–17, Jan. 2021.

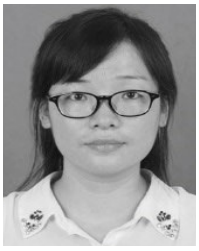

XIAOLING CHEN received the M.S. degree in control theory and application from East China Jiaotong University, in 2015. She is currently a Teacher with the School of Electrical and Information Engineering, Hubei University of Science and Technology. She has published several international journals. Her research interests include surface plasmon photonics of graphene and research on optical artificial supernormal materials.

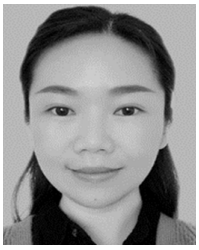

PU ZHANG received the M.S. degree in applied mathematics from the Huazhong University of Science and Technology, in 2007. She is currently an Associate Professor with the School of Education, Hubei University of Science and Technology. Her research interest includes micro nano photonics. In particular, she is very interested in the study of non-Hermitian optical properties of surface plasmon polaritons.

DONG ZHONG (Member, IEEE) received the Ph.D. degree in communication and information system from the Wuhan University of Technology, in 2015. He is currently a Professor with the School of Electrical and Information Engineering, Hubei University of Science and Technology. He has published more than 70 scientific research papers and has presided more than 40 projects. He holds more than ten national invention patents. His research interest includes micro nano photonics.

JUNJIE DONG received the M.S. degree in signal information processing from Chang'an University, in 2014. He is currently a Researcher with the Laboratory of Optoelectronic Information and Intelligent Control, Hubei University of Science and Technology. His research interest includes micro nano photonics.